Supplemental material: Ground State and Hidden Symmetry of Magic Angle Graphene at Even Integer Filling

Nick Bultinck,[1,*] Eslam Khalaf,[2,*] Shang Liu,[2] Shubhayu Chatterjee,[1] Ashvin Vishwanath,[2] and Michael P. Zaletel[1,†]

[1]*Department of Physics, University of California, Berkeley, CA 94720, USA*
[2]*Department of Physics, Harvard University, Cambridge, Massachusetts 02138, USA*

(Dated: July 6, 2020)

CONTENTS

I. HAMILTONIAN

A. Bistritzer-Macdonald model

Our starting point is the Bistritzer-MacDonald (BM) model of the TBG band structure [1], which we now briefly review. We begin with two layers of perfectly aligned (AA stacking) graphene sheets extended along the xy plane, and we choose the frame orientation such that the y-axis is parallel to some of the honeycomb lattice bonds. Now we choose an arbitrary atomic site and twist the top and bottom layers around that site by the counterclockwise angles $\theta/2$ and $-\theta/2$ (say $\theta > 0$), respectively. When θ is very small, the lattice form a Moiré pattern with very large translation vectors; correspondingly, the Moiré Brillouin zone (MBZ) is very small compared to the monolayer graphene Brillouin zone (BZ). In this case, coupling between the two valleys can be neglected. If we focus on one of the two valleys, say K, then the effective Hamiltonian is given by:

$$\mathcal{H}_S = \sum_l \sum_{\boldsymbol{k}} f_l^\dagger(\boldsymbol{k}) h_{\boldsymbol{k}}(l\theta/2) f_l(\boldsymbol{k}) + \left(\sum_{\boldsymbol{k}} \sum_{j=1}^{3} f_t^\dagger(\boldsymbol{k}+\boldsymbol{q}_j) T_j f_b(\boldsymbol{k}) + h.c. \right). \tag{S1}$$

* N. Bultinck and E. Khalaf contributed equally to this work.
† mikezaletel@berkeley.edu

Here, $l = t/b$ is the layer index, and $f_l(\boldsymbol{k})$ is the K-valley electron originated from layer l. The sublattice index σ is suppressed, thus each $f_l(\boldsymbol{k})$ operator is in fact a two-column vector. In the original BM model, $h_{\boldsymbol{k}}(\theta)$ is the linearized monolayer graphene K-valley Hamiltonian with twist angle θ:

$$h_{\boldsymbol{k}}(\theta) = \hbar v_F(k_x\sigma_x + k_y\sigma_y)e^{-i\theta\sigma_z} \tag{S2}$$

where v_F is the Fermi velocity. In our numerics, we do not use the linearized dispersion (S2), but we replace it with the complete mono-layer graphene Hamiltonian. This means that $h_{\boldsymbol{k}}(\theta)$ is instead given by

$$h_{\boldsymbol{k}}(\theta) = h_{MLG}(\boldsymbol{K} + R(\theta)\boldsymbol{k}) = \begin{pmatrix} 0 & g_0(\boldsymbol{K} + R(\theta)\boldsymbol{k}) \\ g_0^*(\boldsymbol{K} + R(\theta)\boldsymbol{k}) & 0 \end{pmatrix}, \tag{S3}$$

where $R(\theta)$ is the two-dimensional rotation matrix which rotates over an angle θ, $g_0(\boldsymbol{k})$ is given by

$$g_0(\boldsymbol{k}) = -t_0 \sum_{l=1}^{3} e^{i\boldsymbol{k}\cdot\boldsymbol{\delta}_l}, \tag{S4}$$

and $\boldsymbol{\delta}_l$ are the three vectors connecting an A-sublattice site to its neighboring B-sublattice sites.

To define the second term in the BM Hamiltonian (S1) describing the inter-layer tunneling, we write the K-vector of layer l as K_l. With this notation, $\boldsymbol{q}_1$ is defined as $K_b - K_t$. $\boldsymbol{q}_2 = O_3\boldsymbol{q}_1$ is the counterclockwise 120° rotation of $\boldsymbol{q}_1$, and $\boldsymbol{q}_3 = O_3\boldsymbol{q}_2$. Finally, the three matrices T_i are given by

$$T_j = w_0\sigma_0 + w_1\sigma_x e^{\frac{2\pi i}{3}(j-1)\sigma_z} \tag{S5}$$

Unless otherwise stated, we will use the values

$$t_0 = 2.8\,\text{eV}, \qquad w_0 = 80\,\text{meV}, \qquad w_1 = 110\,\text{meV}, \qquad \theta = 1.05^o \tag{S6}$$

The single particle Hamiltonian within each valley $\mathcal{H}_\pm$ is invariant under the following symmetries

$$C_3 f_{\boldsymbol{k}} C_3^{-1} = e^{-\frac{2\pi}{3}i\tau_z\sigma_z} f_{C_3\boldsymbol{k}}, \quad (C_2\mathcal{T})f_{\boldsymbol{k}}(C_2\mathcal{T})^{-1} = \sigma_x f_{\boldsymbol{k}}, \qquad \mathcal{M}_y f_{\boldsymbol{k}} M_y^{-1} = \sigma_x\mu_x f_{M_y\boldsymbol{k}}, \tag{S7}$$

where $M_y\boldsymbol{k} = (k_x, -k_y)$. In addition, the two valleys are related by time-reversal symmetry given by

$$\mathcal{T} f_{\boldsymbol{k}} \mathcal{T}^{-1} = \tau_x f_{-\boldsymbol{k}}. \tag{S8}$$

Here, $\boldsymbol{\sigma}, \boldsymbol{\tau}$ and $\boldsymbol{\mu}$ denote the Pauli matrices in sublattice, valley and layer spaces, respectively. As a result, we can also write C_2 as

$$C_2 f_{\boldsymbol{k}} C_2^{-1} = \tau_x\sigma_x f_{-\boldsymbol{k}} \tag{S9}$$

In addition, at small angles, we can neglect the θ dependence of $h_{\boldsymbol{k}}(\theta)$. In this case, we have the extra unitary particle-hole symmetry given by

$$\mathcal{P} f_{\boldsymbol{k}} \mathcal{P}^{-1} = i\sigma_x\mu_y f_{-\boldsymbol{k}}^\dagger \tag{S10}$$

In addition, we have $U_V(1)$ valley charge conservation given by

$$U_V f_{\boldsymbol{k}} U_V^{-1} = e^{i\phi\tau_z} f_{\boldsymbol{k}} \tag{S11}$$

For the first-quantized Hamiltonian, the symmetries can be written as illustrated in Table I. Here, we made the replacement $\mathcal{M} \to i\mathcal{M}$ whenever necessary to make all $\mathbb{Z}_2$ unitary symmetries square to $+1$ and $[\mathcal{T}, \mathcal{P}] = 0$.

	$w_0 \neq 0$					$w_0 = 0$	
	$\mathcal{T}$	C_2	$C_2\mathcal{T}$	$\mathcal{P}$	$\mathcal{PT}$	$\mathcal{S}$	$R = \mathcal{SPT}$
Original basis	$\tau_x\mathcal{K}$	$\tau_x\sigma_x$	$\sigma_x\mathcal{K}$	$i\sigma_x\mu_y\mathcal{K}$	$\tau_x\sigma_x\mu_y$	σ_z	$\tau_x\sigma_y\mu_y$
Sublattice basis	$\tau_x\mathcal{K}$	$\sigma_x\tau_x e^{i\theta(\boldsymbol{k})}$	$e^{i\theta(\boldsymbol{k})}\sigma_x\mathcal{K}$	$\tau_z\sigma_y\mathcal{K}$	$\tau_y\sigma_y$	σ_z	$\tau_y\sigma_x$

TABLE I. Symmetries of the BM model with non-vanishing/vanishing intrasublattice hopping in the original microscopic basis and the projected sublattice basis. In the latter, the gauge is chosen such that $\mathcal{T} = \tau_x\mathcal{K}$ and $P = \tau_z\sigma_y\mathcal{K}$ and $\mathcal{K}$. Here, τ, σ, μ, γ denote the Pauli matrices in the valley, sublattice, layer and band, respectively.

B. Chiral model

The chiral limit corresponds to taking the limit of vanishing intrasublattice Moire hopping $w_0 = 0$. In this case, the Hamiltonian has the extra anti-unitary chiral symmetry

$$\mathcal{S} f_{\boldsymbol{k}} \mathcal{S}^{-1} = \sigma_z f^\dagger_{\boldsymbol{k}} \tag{S12}$$

In this case, we can perform the gauge transformation $f_{l,\boldsymbol{k}} \mapsto e^{\frac{i}{2}l\theta\sigma_z} f_{l,\boldsymbol{k}}$ to get rid of the θ dependence in the first term in the Hamiltonian. As a result, the particle-hole symmetry (S10) is exact at all angles. This means that we can combine $\mathcal{S}$, $\mathcal{T}$ and $\mathcal{P}$ to get a $\mathbb{Z}_2$ unitary symmetry $R = \mathcal{SPT}$

$$R f_{\boldsymbol{k}} R^{-1} = \tau_x\sigma_y\mu_y f_{\boldsymbol{k}} \tag{S13}$$

which flips layer, valley and sublattice. Combining this symmetry with the different symmetries of the model, we can generate different versions of the symmetries, for example new time-reversal symmetry $\mathcal{T}' = \mathcal{T}U$ acting as

$$\mathcal{T}' f_{\boldsymbol{k}} \mathcal{T}'^{-1} = \sigma_y\mu_y f_{-\boldsymbol{k}} \tag{S14}$$

This time-reversal symmetry flips layer and sublattice indices but acts within the same valley. We can also define a new C_2 symmetry $C_2' = C_2U$ which leaves valley and sublattice index invariant

$$C_2' f_{\boldsymbol{k}} C_2'^{-1} = \sigma_z\mu_y f_{-\boldsymbol{k}} \tag{S15}$$

In addition, we can combine $\mathcal{T}'$ with C_2 to get a new $C_2\mathcal{T}$ symmetry which leaves momentum invariant but interchanges valley and sublattice

$$(C_2\mathcal{T}') f_{\boldsymbol{k}} (C_2\mathcal{T}')^{-1} = i\tau_x\mu_y\sigma_z f_{\boldsymbol{k}} \tag{S16}$$

which satisfies $(C_2\mathcal{T}')^2 = -1$.

C. Interaction and projection onto active bands

In the following, we derive the form of the interaction when projecting onto a set of active bands. Let $c^\dagger_\alpha(\boldsymbol{k})$ be the creation operator for the energy eigenstate labelled by the combined index $\alpha = (\mu, n)$ which includes the flavor index μ labelled by spin $s = \uparrow, \downarrow$ and valley $\tau = \pm$ and band index n. The fermion creation operator $f^\dagger_{\mu,a}(\boldsymbol{r})$, with a denoting the layer and sublattice indices $a = (l, \sigma)$, in the continuum model is defined by expanding the graphene lattice fermion creation operator close to the K and K' points as $f^\dagger_{s,\sigma,l}(\boldsymbol{r}) = e^{i\boldsymbol{K}_l\cdot\boldsymbol{r}} f^\dagger_{(s,\tau=+),a}(\boldsymbol{r}) + e^{-i\boldsymbol{K}_l\cdot\boldsymbol{r}} f^\dagger_{(s,\tau=-),a}(\boldsymbol{r})$. $f^\dagger_{\mu,a}(\boldsymbol{q})$ is its Fourier transform in terms of the continuous momentum $\boldsymbol{q}$ which is not restricted within the first Moiré Brillouin zone. $c^\dagger$ and $f^\dagger$ are related to each other by the k-space wave functions as follows:

$$c^\dagger_{\mu,n}(\boldsymbol{k}) = \sum_{\boldsymbol{G},a} u_{\tau,n;\boldsymbol{G},a}(\boldsymbol{k}) f^\dagger_{\mu,a}(\boldsymbol{k} + \boldsymbol{G}), \tag{S17}$$

where $\boldsymbol{G}$ is a Moiré reciprocal lattice vector and we used the fact that the wave functions are spin-independent. Once we choose a gauge of $u_{\tau,n;\boldsymbol{G},a}(\boldsymbol{k})$ for all $\boldsymbol{k}$ in some MBZ, $c^\dagger(\boldsymbol{k})$ are defined in terms of the $f^\dagger(\boldsymbol{q})$ for those $\boldsymbol{k}$. Due to the band topology, it is generally impossible to choose a symmetric, smooth and periodic gauge [2–5]. We will generally always choose the gauge to

be symmetric which means that it is either singular/discontinuous or not periodic. In general, this means that

$$u_{\tau,n;\boldsymbol{G},a}(\boldsymbol{k}+\boldsymbol{G}_0)=\sum_m [U_{\tau,\boldsymbol{G}_0}(\boldsymbol{k})]_{mn}u_{\tau,m;\boldsymbol{G}+\boldsymbol{G}_0,a}(\boldsymbol{k}),\qquad U_{\tau,\boldsymbol{G}_0}(\boldsymbol{k})^\dagger U_{\tau,\boldsymbol{G}_0}(\boldsymbol{k})=1 \tag{S18}$$

where $U_{\tau,\boldsymbol{G}}(\boldsymbol{k})=1$ for any periodic gauge. This, in turn, implies

$$c^\dagger(\boldsymbol{k}+\boldsymbol{G})=U_{\boldsymbol{G}}(\boldsymbol{k})c^\dagger(\boldsymbol{k}),\qquad U_{\boldsymbol{G}}(\boldsymbol{k})=\mathrm{diag}(U_{+,\boldsymbol{G}}(\boldsymbol{k}),U_{-,\boldsymbol{G}}(\boldsymbol{k}))_\tau \tag{S19}$$

Note that the momentum argument for $f^\dagger$ is unconstrained since we are using the continuum theory for monolayers of graphene and the normalization is chosen such that $\{f_{\mu,a}(\boldsymbol{q}),f^\dagger_{\mu',a'}(\boldsymbol{q}')\}=\delta_{\mu\mu'}\delta_{aa'}\delta_{\boldsymbol{q}\boldsymbol{q}'}$ (suppose the system size is finite), and $\langle u_{\tau,n}(\boldsymbol{k})|u_{\tau',n'}(\boldsymbol{k})\rangle=\delta_{\tau\tau'}\delta_{nn'}$, which imply $\{c_{\mu,n}(\boldsymbol{k}),c^\dagger_{\mu',n'}(\boldsymbol{k}')\}=\delta_{\mu\mu'}\delta_{nn'}\delta_{\boldsymbol{k}\boldsymbol{k}'}$ when $\boldsymbol{k},\boldsymbol{k}'$ are confined in the MBZ. For the purpose of projecting the interaction into these two bands, it is convenient to introduce the form factor matrix

$$[\Lambda_{\boldsymbol{q}}(\boldsymbol{k})]_{\alpha,\beta}:=\langle u_\alpha(\boldsymbol{k})|u_\beta(\boldsymbol{k}+\boldsymbol{q})\rangle \tag{S20}$$

It follows from the definition that the form factor satisfies

$$\Lambda_{\boldsymbol{q}}(\boldsymbol{k})^\dagger=\Lambda_{-\boldsymbol{q}}(\boldsymbol{k}+\boldsymbol{q}),\qquad \Lambda_{\boldsymbol{q}}(\boldsymbol{k}+\boldsymbol{G})=U^*_{\boldsymbol{G}}(\boldsymbol{k})\Lambda_{\boldsymbol{q}}(\boldsymbol{k})U^T_{\boldsymbol{G}}(\boldsymbol{k}+\boldsymbol{q}) \tag{S21}$$

The interacting Hamiltonian is given by

$$\mathcal{H}_{\mathrm{int}}=\sum_{\boldsymbol{k}}c^\dagger(\boldsymbol{k})h(\boldsymbol{k})c(\boldsymbol{k})+\frac{1}{2A}\sum_{\boldsymbol{q}}V(\boldsymbol{q}):\rho_{\boldsymbol{q}}\rho_{-\boldsymbol{q}}:,\qquad \rho_{\boldsymbol{q}}=\sum_{\boldsymbol{k}}c^\dagger(\boldsymbol{k})\Lambda_{\boldsymbol{q}}(\boldsymbol{k})c(\boldsymbol{k}+\boldsymbol{q}) \tag{S22}$$

where A is the total area of the system and $V(\boldsymbol{q})$ is the momentum space interaction potential, related to the real-space one by $V(\boldsymbol{q}):=\int d^2\boldsymbol{r}V(\boldsymbol{r})e^{-i\boldsymbol{q}\cdot\boldsymbol{r}}$ and $h(\boldsymbol{k})$ includes both the single-particle BM Hamiltonian as well as band renormalization effects due to remote bands not included in the projection. Depending on the number of gates, $V(\boldsymbol{q})$ takes the following form in the SI units:

$$V(\boldsymbol{q})=\frac{e^2}{2\epsilon\epsilon_0 q}\begin{cases}(1-e^{-2qd_s}), & \text{(single-gate)}\\ \tanh(qd_s), & \text{(dual-gate)}\end{cases} \tag{S23}$$

where the screening length d_s is the distance from the graphene plane to the gate(s). Unless otherwise stated, we will use the double-gate-screened expression with $\epsilon=9.5$ and $d_s=40$nm.

II. HARTREE-FOCK

Here we detail our implementation of the Hartree-Fock method, in particular our "subtraction" scheme for avoiding a double-counting of the mean-field interaction, and our prescription for projecting onto a finite number of bands. Modulo a soon-to-be-discussed correction, the Hamiltonian is

$$\mathcal{H}_{\mathrm{eff}}=\sum_{\boldsymbol{k}\in\mathrm{BZ}}c^\dagger_{\boldsymbol{k}}h_{\mathrm{BM}}(\boldsymbol{k})c_{\boldsymbol{k}}+\frac{1}{2A}\sum_{\boldsymbol{q}}V_{\boldsymbol{q}}:\rho_{\boldsymbol{q}}\rho_{-\boldsymbol{q}}:, \tag{S24}$$

$$\rho_{\boldsymbol{q}}=\sum_{\boldsymbol{k}\in\mathrm{BZ}}c^\dagger_{\boldsymbol{k}}\Lambda_{\boldsymbol{q}}(\boldsymbol{k})c_{\boldsymbol{k}+\boldsymbol{q}},\quad [\Lambda_{\boldsymbol{q}}(\boldsymbol{k})]_{\alpha,\beta}=\langle u_{\alpha,\boldsymbol{k}}|u_{\beta,\boldsymbol{k}+\boldsymbol{q}}\rangle \tag{S25}$$

where h_{BM} is the BM-Hamiltonian, with eigenstates labelled by α. For the numerical calculations, we find it convenient to adopt a periodic gauge which means –using the notation of the previous appendix– that $U_{\boldsymbol{G}}(\boldsymbol{k})=\mathbb{1}$ (note that in our analytical discussions we sometimes use a different gauge, namely a symmetric one).

Given a Slater determinant with correlation matrix $P_{\alpha\beta}(\boldsymbol{k})=\langle c^\dagger_{\alpha,\boldsymbol{k}}c_{\beta,\boldsymbol{k}}\rangle$, the corresponding Coulomb contribution to the Hartree-Fock Hamiltonian is

$$H^{\mathrm{C}}_{\mathrm{MF}}[P](\boldsymbol{k})=\frac{1}{A}\sum_{\boldsymbol{G}}V_{\boldsymbol{G}}\Lambda_{\boldsymbol{G}}(\boldsymbol{k})\sum_{\boldsymbol{k}'\in\mathrm{BZ}}\mathrm{tr}\left(P(\boldsymbol{k}')\Lambda^*_{\boldsymbol{G}}(\boldsymbol{k}')\right)-\frac{1}{A}\sum_{\boldsymbol{q}}V_{\boldsymbol{q}}\Lambda_{\boldsymbol{q}}(\boldsymbol{k})P^T(\boldsymbol{k}+\boldsymbol{q})\Lambda^\dagger_{\boldsymbol{q}}(\boldsymbol{k})\,, \tag{S26}$$

so that the total energy of this state is given by

$$E_{\rm MF} = \sum_{\boldsymbol{k}} \text{tr}\left(P(\boldsymbol{k})(h_{\rm BM}(\boldsymbol{k}) + \frac{1}{2} H^{\rm C}_{\rm MF}[P](\boldsymbol{k}))^T \right) \tag{S27}$$

However, as pointed out in Ref. [6], if the parameters of $h_{\rm BM}$ are obtained by a method such as DFT, or by comparison with experiment, then $h_{\rm BM}$ will already contain, to some extent, the effect of the interactions, and the above expression will double-count this contribution. Consider, for example, the case where the two layers are decoupled, so that $h_{\rm BM}$ is two copies of graphene. If we take for $P(\boldsymbol{k})$ the ground state of graphene at neutrality, then the Fock contribution to $H^{\rm C}_{\rm MF}[P]$ will lead to a logarithmically divergent renormalization of the Dirac velocity. However, the tight-binding parameters $h_{\rm BM}$ are already chosen to replicate the measured Dirac velocity, so this renormalization will be unphysical.

To remedy this, it was suggested that the BM Hamiltonian should be replaced by $h(\boldsymbol{k}) = h_{\rm BM} - \frac{1}{2} H^{\rm C}_{\rm MF}[P^0](\boldsymbol{k})$, where P^0 is a "reference" density matrix such that $h_{\rm BM}$ is the full effective Hamiltonian when $P = P^0$. The choice of P^0 then in principle depends on the method used to derive $h_{\rm BM}$. As in Ref. [7], we choose P^0 to be the density matrix of two decoupled graphene layers at neutrality. While it may be tempting to choose P^0 to be the density matrix of $h_{\rm BM}$ at neutrality, in most ab-initio methods [8] the parameters in $h_{\rm BM}$ are obtained without any reference to the twist angle θ, so it wouldn't make sense for P^0 to then depend on θ.

Having chosen P^0, we must truncate to a finite number of bands for computational purposes. We truncate based on projection into the eigenbasis α of $h_{\rm BM}$, choosing $4N_- \leq \alpha \leq 4N_+$ of the bands closest to the flat bands (N_- and N_+ denote the number of bands per spin and valley). We assume that below / above $4N_-/4N_+$ the density matrix is empty / full, e.g. $P_{\alpha\beta}(\boldsymbol{k}) = \delta_{\alpha\beta}$ for $\alpha, \beta < 4N_-$ and $P_{\alpha\beta}(\boldsymbol{k}) = 0$ for $\alpha, \beta > 4N_+$, while for $4N_- \leq \alpha, \beta \leq 4N_+$, $P_{\alpha\beta}(\boldsymbol{k})$ is determined by HF. In principle, this implies the HF Hamiltonian includes a contribution from all the filled bands $\alpha < N_-$. However, there is also the corresponding subtraction of the reference density matrix $P^0_{\alpha\beta}$. Because of the small inter-layer tunneling $w \sim 100$ meV, the contributions from $P_{\alpha\alpha}$ and $P^0_{\alpha\alpha}$ cancel out for α corresponding to bands far away from the charge neutrality point.

With the subtraction of the reference density matrix P^0 taken into account, the Hartree-Fock mean field Hamiltonian is given by

$$\mathcal{H}_{\rm MF}[P] = \sum_{\boldsymbol{k}} c^\dagger_{\boldsymbol{k}} \left(h(\boldsymbol{k}) + H^C_{\rm MF}[P](\boldsymbol{k}) \right) c_{\boldsymbol{k}} - \frac{1}{2} \sum_{\boldsymbol{k}} \text{tr}\left(H^C_{\rm MF}[P](\boldsymbol{k}) P(\boldsymbol{k})^T \right) \tag{S28}$$

The zero-temperature Hartree-Fock self-consistency condition states that the correlation matrix of the ground-state Slater determinant of $\mathcal{H}_{MF}[P]$ should be given by $P(\boldsymbol{k})$. To numerically solve the self-consistency equation we used both the 'ODA' and 'EDIIS' algorithms, both of which are developed and explained in detail in Refs. [9, 10].

III. FLAT BAND PROJECTED HAMILTONIAN

Motivated by the numerical observation that mixing between the two flat bands and the remaining bands is relatively small for symmetry-broken phases at CN, we will only keep these two bands in the following discussion. The effect of the other bands will be included only through renormalization effects of the single-particle Hamiltonian $h(\boldsymbol{k})$ following the scheme of Ref. [6].

A. Sublattice-polarized basis

In the chiral limit $w_0 = 0$, the sublattice operator σ_z anticommutes with the BM Hamiltonian leaving the space of states spanning the flat bands invariant. Thus, we can choose the flat band states to be eigenstates of the sublattice operator σ_z. This basis is distinct from the band basis where the chiral symmetry operator is off-diagonal since it maps positive energy states to negative energy states. We note that the sublattice basis remains well-defined in the flat band limit for which the band basis is not well-defined.

Away from the chiral limit, we can still define the sublattice basis by diagonalizing the operator $\Gamma_{nm}(\boldsymbol{k}) = \langle u_n(\boldsymbol{k}) | \sigma_z | u_m(\boldsymbol{k}) \rangle$. This yields a well-defined basis as long as the eigenvalues of $\Gamma(\boldsymbol{k})$ (which have equal magnitude and opposite sign due to $C_2\mathcal{T}$) are non-zero, indicating a finite sublattice polarization. The sublattice polarization given by $\sqrt{|\det \Gamma(\boldsymbol{k})|}$ is plotted in the left panel of Fig. S1 for the realistic model parameters (S6) and we can see it never goes to zero. This can also be seen in the right panel where the minimum and average value of sublattice polarization over the Moiré Brillouin zone is plotted as a function of w_0/w_1. We can clearly see from the plot that this value never geso to zero showing that the sublattice-polarized wavefunctions, those which diagonalize σ_z, for the realistic model are adiabatically connected to those of the chiral model. As in the main text, we will use the same Pauli matrices $\boldsymbol{\sigma}$ both sublattice index and the band index for sublattice-polarized wave-functions. It should

be noted, however, that for $w_0 \neq 0$, the wavefunctions labelled by $\boldsymbol{\sigma}$ are only partially polarized on one of the sublattices i.e. they have amplitude on both sublattices. We note that for the chiral model at the magic angle, the sublattice-polarized wavefunctions have an explicit form in terms of theta functions given in Ref. [11].

To obtain the implementation of the different symmetries we start by noting that the eigenstates for a given spin can be labelled by their eigenvalues under τ_z (valley index) and σ_z (sublattice index). The phases of the four different wavefunctions can be chosen arbitrarily. Such choices will affect the form of the remaining symmetries in this basis. Once the phase of the wavefunction in valley K, sublattice A is fixed, we can use two of the three symmetries C_2, $\mathcal{T}$ and $\mathcal{P}$ (or some combinations of them) to fix the phase for the other three wavefunctions. Since we will be mostly using time-reversal and particle-hole symmetries, we will choose to fix these as

$$\mathcal{T} = \tau_x \mathcal{K}, \qquad \mathcal{P} = \tau_z \sigma_y \mathcal{K} \tag{S29}$$

which are chosen such that $\mathcal{T}$ flips valley but not sublattice ($\{\mathcal{T}, \tau_z\} = 0$, $[\mathcal{T}, \sigma_z] = 0$) and $\mathcal{P}$ flips sublattice but not valley ($\{P, \sigma_z\} = 0$, $[\mathcal{P}, \tau_z] = 0$). This leads to simple forms for $\mathcal{PT}$ and R symmetries

$$\mathcal{PT} = \tau_y \sigma_y, \qquad R = \tau_y \sigma_x \tag{S30}$$

Once these operators are fixed, we are not free to choose the form of C_2, e.g. $\sigma_x \tau_x$. To see this, consider the modified two-fold rotation symmetry $C_2' = i\tau_z C_2 R$ which is diagonal in sublattice, $[C_2', \sigma_z] = 0$, and valley, $[C_2', \tau_z] = 0$, and commutes with R and $\mathcal{T}$. As a result, $C_2' = e^{i\theta(\boldsymbol{k})}$ for some angle $\theta(\boldsymbol{k})$ satisfying $\theta(-\boldsymbol{k}) = -\theta(\boldsymbol{k})$. Thus, $\theta(\boldsymbol{k}) = 0, \pi$ at any TRIM (Γ, M, M' and M''). We now note that sublattice-polarized badns has Chern number ± 1 which implies that the sum of $\theta(\boldsymbol{k})$ over all TRIMs should be an odd multiple of π [12]. As a result, $\theta(\boldsymbol{k})$ cannot be constant over the Brillouin zone and has to have non-trivial $\boldsymbol{k}$-dependence. The representation of C_2 in the same basis can be easily obtained as

$$C_2 = \sigma_x \tau_x e^{i\theta(\boldsymbol{k})} \tag{S31}$$

The symmetry representations in the sublattice-polarized basis in the chosen gauge are summarized in Table I.

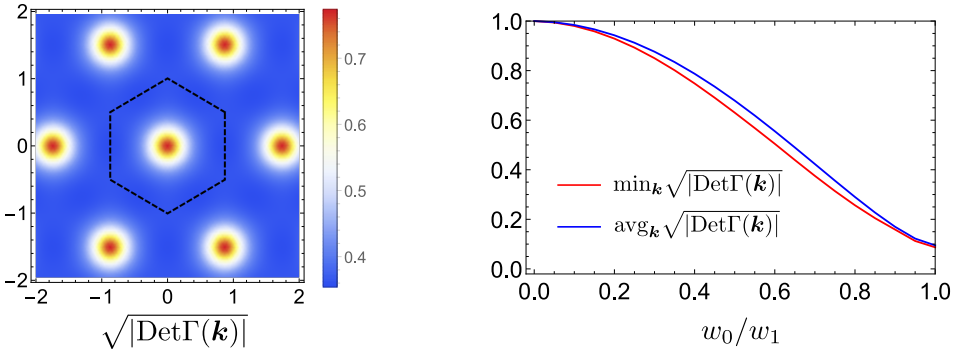

FIG. S1. Left panel shows the value of sublattice polarization computed by projecting the sublattice operator σ_z on the flat band as a function of $\boldsymbol{k}$ for the realistic parameters (S6). Right panel shows the minimum and average value of the sublattice polarization as a function of the ratio w_0/w_1. We can see that it never goes to zero indicating that the sublattice-polarized wavefunctions for the realistic model are adiabatically connected to those of the chiral model.

B. Properties of the form factors

Let us start with decomposing the form factor into parts which commutes/anticommute with the chiral symmetry σ_z

$$\Lambda_{\boldsymbol{q}}(\boldsymbol{k}) = \Lambda^S_{\boldsymbol{q}}(\boldsymbol{k}) + \Lambda^A_{\boldsymbol{q}}(\boldsymbol{k}), \qquad \Lambda^{S/A}_{\boldsymbol{q}}(\boldsymbol{k}) = \frac{1}{2}(\Lambda_{\boldsymbol{q}}(\boldsymbol{k}) \pm \sigma_z \Lambda_{\boldsymbol{q}}(\boldsymbol{k}) \sigma_z) \tag{S32}$$

In the chiral limit, the space of flat bands is invariant under chiral symmetry leading to vanishing $\Lambda^A_{\boldsymbol{q}}(\boldsymbol{k})$.

Let us now see what is the most general form of $\Lambda^{S/A}_{\boldsymbol{q}}(\boldsymbol{k})$ deduced from the other symmetries. $\mathrm{U}(2)_K \times \mathrm{U}(2)_{K'}$ imply that $\Lambda_{\boldsymbol{q}}(\boldsymbol{k})$ is diagonal in valley and independent of spin, limiting it to the terms $\tau_{0,z}\sigma_{0,x,y,z}$. $\mathcal{PT}$ symmetry further restricts these to $\tau_0\sigma_{0,y}$ and $\tau_z\sigma_{x,z}$ whereas $C_2\mathcal{T}$ enforces the term multiplying $\tau_z\sigma_z$ to be purely imaginary and the remaining terms to be purely

real, leading to

$$\Lambda^S_{\boldsymbol{q}}(\boldsymbol{k}) = F^S_{\boldsymbol{q}}(\boldsymbol{k}) e^{i\Phi^S_{\boldsymbol{q}}(\boldsymbol{k})\sigma_z\tau_z}, \quad \Lambda^A_{\boldsymbol{q}}(\boldsymbol{k}) = \sigma_x\tau_z F^A_{\boldsymbol{q}}(\boldsymbol{k}) e^{i\Phi^A_{\boldsymbol{q}}(\boldsymbol{k})\sigma_z\tau_z}, \tag{S33}$$

In addition, $\mathcal{T}$ implies

$$F^S_{-\boldsymbol{q}}(-\boldsymbol{k}) = F^S_{\boldsymbol{q}}(\boldsymbol{k}), \quad \Phi^S_{-\boldsymbol{q}}(-\boldsymbol{k}) = \Phi^S_{\boldsymbol{q}}(\boldsymbol{k}), \quad F^A_{-\boldsymbol{q}}(-\boldsymbol{k}) = -F^A_{\boldsymbol{q}}(\boldsymbol{k}), \quad \Phi^A_{-\boldsymbol{q}}(-\boldsymbol{k}) = \Phi^A_{\boldsymbol{q}}(\boldsymbol{k}) \tag{S34}$$

C. Hierarchy of scales

1. *Particle-hole symmetric Hamiltonian*

The full Hamiltonian is given by (S22) where $h(\boldsymbol{k})$ is the renormalized single-particle dispersion. That is, the dispersion when the flat bands are completely empty, i.e. $\nu = -4$. This can be written in terms of the dispersion at charge neutrality as

$$h(\boldsymbol{k}) = h_{\nu=0}(\boldsymbol{k}) - \frac{1}{A}\sum_{\boldsymbol{G}} V_{\boldsymbol{G}} \Lambda_{\boldsymbol{G}}(\boldsymbol{k}) \sum_{\boldsymbol{k}'} \operatorname{tr} P_0(\boldsymbol{k}') \Lambda^*_{\boldsymbol{G}}(\boldsymbol{k}') + \frac{1}{A}\sum_{\boldsymbol{q}} V_{\boldsymbol{q}} \Lambda_{\boldsymbol{q}}(\boldsymbol{k}) P_0^T(\boldsymbol{k}+\boldsymbol{q}) \Lambda^\dagger_{\boldsymbol{q}}(\boldsymbol{k}) \tag{S35}$$

This expression assumed a periodic gauge such that $\Lambda_{\boldsymbol{G}}(\boldsymbol{k})^\dagger = \Lambda_{-\boldsymbol{G}}(\boldsymbol{k})$. Here, we have assumed there is always a solution to the HF equations at charge neutrality $\nu = 0$ which does not break any symmetry, with the self-consistent HF dispersion denoted by $h_{\nu=0}(\boldsymbol{k})$ and the projection onto the filled bands denoted by P_0. It can be numerically checked that such solution reproduces to a very good approximation the projection of the BM Hamiltonian on the two flat bands as suggested in Ref. [6]. $\mathrm{U}_V(1)$, $C_2\mathcal{T}$ and $\mathcal{PT}$ imply that $h_{\nu=0}$ has the form

$$h_{\nu=0}(\boldsymbol{k}) = a(\boldsymbol{k})\tau_z + f(\boldsymbol{k})\sigma_x e^{i\phi_0(\boldsymbol{k})\sigma_z\tau_z} \tag{S36}$$

which leads to

$$P_0(\boldsymbol{k}) = \frac{1}{2}[1 + Q_0(\boldsymbol{k})], \qquad Q_0(\boldsymbol{k}) = \sigma_x e^{i\phi_0(\boldsymbol{k})\sigma_z\tau_z} \tag{S37}$$

Substituting in (S35), we get

$$h(\boldsymbol{k}) = h_{\mathrm{BM}}(\boldsymbol{k}) - \frac{1}{2A}\sum_{\boldsymbol{G}} V_{\boldsymbol{G}} \Lambda_{\boldsymbol{G}}(\boldsymbol{k}) \sum_{\boldsymbol{k}'} \operatorname{tr} \Lambda^*_{\boldsymbol{G}}(\boldsymbol{k}') + \frac{1}{2A}\sum_{\boldsymbol{q}} V_{\boldsymbol{q}} \Lambda_{\boldsymbol{q}}(\boldsymbol{k}) \Lambda^\dagger_{\boldsymbol{q}}(\boldsymbol{k}) + \frac{1}{2A}\sum_{\boldsymbol{q}} V_{\boldsymbol{q}} \Lambda_{\boldsymbol{q}}(\boldsymbol{k}) Q_0(\boldsymbol{k}+\boldsymbol{q}) \Lambda^\dagger_{\boldsymbol{q}}(\boldsymbol{k}) \tag{S38}$$

where we used the fact that $\operatorname{tr} Q_0(\boldsymbol{k})\Lambda^*_G(\boldsymbol{k})$ vanishes due to the form of $\Lambda_{\boldsymbol{q}}(\boldsymbol{k})$ given in (S32) and (S33). Substituting in the interaction Hamiltonian, we get

$$\mathcal{H}_{\mathrm{int}} = \sum_{\boldsymbol{k}} c^\dagger_{\boldsymbol{k}} \tilde{h}(\boldsymbol{k}) c_{\boldsymbol{k}} + \frac{1}{2A}\sum_{\boldsymbol{q}} V_{\boldsymbol{q}} \delta\rho_{\boldsymbol{q}} \delta\rho^\dagger_{-\boldsymbol{q}} + \text{const.} \tag{S39}$$

$$\tilde{h}(\boldsymbol{k}) = h_{\nu=0}(\boldsymbol{k}) + \frac{1}{2A}\sum_{\boldsymbol{q}} V_{\boldsymbol{q}} \Lambda_{\boldsymbol{q}}(\boldsymbol{k}) Q_0(\boldsymbol{k}+\boldsymbol{q}) \Lambda^\dagger_{\boldsymbol{q}}(\boldsymbol{k}), \qquad \delta\rho_{\boldsymbol{q}} = \rho_{\boldsymbol{q}} - \bar{\rho}_{\boldsymbol{q}}, \qquad \bar{\rho}_{\boldsymbol{q}} = \frac{1}{2}\sum_{\boldsymbol{G},\boldsymbol{k}} \delta_{\boldsymbol{G},\boldsymbol{q}} \operatorname{tr} \Lambda_{\boldsymbol{G}}(\boldsymbol{k}) \tag{S40}$$

To reach this expression, we note that the normal-ordered interaction in (S22) differs from the density-density interaction in (S40) by a bilinear term which cancels exactly against the third term in (S38). In addition, we separated the terms in the sum over $\boldsymbol{q}$ corresponding to a reciprocal lattice vector $\boldsymbol{G}$ and combined it with the second term in (S38). The advantage of this form of the Hamiltonian is that both terms are manifestly particle-hole symmetric.

2. *Estimation of energy scales*

Let us now write

$$\delta\rho_{\boldsymbol{q}} = \delta\rho^S_{\boldsymbol{q}} + \delta\rho^A_{\boldsymbol{q}}, \qquad \delta\rho^{S/A}_{\boldsymbol{q}} = \rho^{S/A}_{\boldsymbol{q}} - \bar{\rho}^{S/A}_{\boldsymbol{q}}, \qquad \rho^{S/A}_{\boldsymbol{q}} = \sum_{\boldsymbol{k}} c^\dagger_{\boldsymbol{k}} \Lambda^{S/A}_{\boldsymbol{q}}(\boldsymbol{k}) c_{\boldsymbol{k}}, \qquad \bar{\rho}^{S/A}_{\boldsymbol{q}} = \frac{1}{2}\sum_{\boldsymbol{k},\boldsymbol{G}} \delta_{\boldsymbol{G},\boldsymbol{q}} \operatorname{tr} \Lambda^{S/A}_{\boldsymbol{G}}(\boldsymbol{k}) \tag{S41}$$

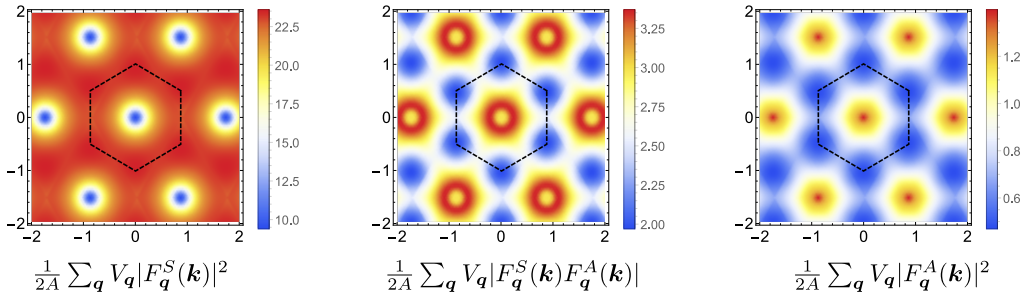

FIG. S2. The energy scale for the symmetry and symmetry breaking terms in the Hamiltonian obtained by averaging the squares of the form factors of the form factor $|F^S_{\boldsymbol{q}}(\boldsymbol{k})|^2$, $F^S_{\boldsymbol{q}}(\boldsymbol{k})F^A_{\boldsymbol{q}}(\boldsymbol{k})$, $|F^A_{\boldsymbol{q}}(\boldsymbol{k})|^2$ over $\boldsymbol{q}$ weighted by the interaction as a function of $\boldsymbol{k}$.

which induces a splitting of the interaction term into a symmetric intrasublattice part (under the unitary symmetry R) and a symmetry breaking intersublattice part given by

$$\mathcal{H}_S = \frac{1}{2A}\sum_{\boldsymbol{q}} V_{\boldsymbol{q}}\delta\rho^S_{\boldsymbol{q}}\delta\rho^S_{-\boldsymbol{q}}, \qquad \mathcal{H}_A = \frac{1}{2A}\sum_{\boldsymbol{q}} V_{\boldsymbol{q}}(\delta\rho^A_{\boldsymbol{q}}\delta\rho^S_{-\boldsymbol{q}} + \delta\rho^S_{\boldsymbol{q}}\delta\rho^A_{-\boldsymbol{q}} + \delta\rho^A_{\boldsymbol{q}}\delta\rho^A_{-\boldsymbol{q}}) \tag{S42}$$

We note here that although $\delta\rho^A\delta\rho^A$ does not by itself break the R symmetry, it is only non-vanishing if this symmetry is broken since otherwise the antisymmetric form factor $\Lambda^A_{\boldsymbol{q}}(\boldsymbol{k})$ vanishes.

One crucial observation is that the magnitude of the symmetric form factor $F^S_{\boldsymbol{q}}(\boldsymbol{k})$ is significantly larger than the magnitude of the antisymmetric form factor $F^S_{\boldsymbol{q}}(\boldsymbol{k})$. This is shown in Fig. S2 where we plot the $\boldsymbol{q}$ average of $|F^S_{\boldsymbol{q}}(\boldsymbol{k})|^2$, $F^S_{\boldsymbol{q}}(\boldsymbol{k})F^A_{\boldsymbol{q}}(\boldsymbol{k})$, $|F^A_{\boldsymbol{q}}(\boldsymbol{k})|^2$ weighted by the interaction. We see that the average values the three terms are about 17, 2 and 0.5 meV, respectively for the parameters in (S6). Although the absolute value of these terms depends on the interaction strength (the chosen value of ϵ), the ratio between them is mostly sensitive to the properties of the wavefunctions close to the magic angle. It is worth noting that these ratios also depends slightly on the screening length as we will discuss later.

The $\boldsymbol{q}$ averaged form factors can be used to define a characteristic scale for $\mathcal{H}_S$ and $\mathcal{H}_A$ by estimating the maximum absolute value of the exchange (Fock energy) as [6]

$$U_S = \frac{1}{2AN}\sum_{\boldsymbol{k},\boldsymbol{q}} V_{\boldsymbol{q}}|F^S_{\boldsymbol{q}}(\boldsymbol{k})|^2, \qquad U_A = \frac{1}{2AN}\sum_{\boldsymbol{k},\boldsymbol{q}} V_{\boldsymbol{q}}\{2|F^S_{\boldsymbol{q}}(\boldsymbol{k})F^A_{\boldsymbol{q}}(\boldsymbol{k})| + |F^A_{\boldsymbol{q}}(\boldsymbol{k})|^2\} \tag{S43}$$

which are plotted in Fig. S2 for the parameters in (S6). By averaging the plotted functions over $\boldsymbol{k}$, we get the values of the bounds U_S and U_A to be 18, and 4.5 meV, respectively, for the choice of parameters (S6).

Similarly, we can split $\tilde{h}(\boldsymbol{k})$ into a symmetric intersublattice part $\propto \sigma_x, \sigma_y\tau_z$ and a symmetry breaking intrasublattice part $\propto \tau_z$ as

$$\tilde{h}(\boldsymbol{k}) = h_0(\boldsymbol{k})\tau_z + h_x(\boldsymbol{k})\sigma_x + h_y(\boldsymbol{k})\sigma_y\tau_z \tag{S44}$$

with

$$\begin{aligned}
h_0(\boldsymbol{k}) &= \frac{1}{8}\operatorname{tr}\tilde{h}(\boldsymbol{k})\tau_z = a(\boldsymbol{k}) + \frac{1}{A}\sum_{\boldsymbol{q}} V_{\boldsymbol{q}}F^S_{\boldsymbol{q}}(\boldsymbol{k})F^A_{\boldsymbol{q}}(\boldsymbol{k})\cos[\phi_0(\boldsymbol{k}) - \Phi^S_{\boldsymbol{q}}(\boldsymbol{k}) - \Phi^A_{\boldsymbol{q}}(\boldsymbol{k})] \\
h_x(\boldsymbol{k}) &= \frac{1}{8}\operatorname{tr}\tilde{h}(\boldsymbol{k})\sigma_x = f(\boldsymbol{k})\cos\phi_0(\boldsymbol{k}) + \frac{1}{A}\sum_{\boldsymbol{q}} V_{\boldsymbol{q}}\{[F^S_{\boldsymbol{q}}(\boldsymbol{k})]^2\cos[\phi_0(\boldsymbol{k}) - 2\Phi^S_{\boldsymbol{q}}(\boldsymbol{k})] + [F^A_{\boldsymbol{q}}(\boldsymbol{k})]^2\cos[\phi_0(\boldsymbol{k}) - 2\Phi^A_{\boldsymbol{q}}(\boldsymbol{k})]\} \\
h_y(\boldsymbol{k}) &= \frac{1}{8}\operatorname{tr}\tilde{h}(\boldsymbol{k})\sigma_y\tau_z = f(\boldsymbol{k})\sin\phi_0(\boldsymbol{k}) + \frac{1}{A}\sum_{\boldsymbol{q}} V_{\boldsymbol{q}}\{[F^S_{\boldsymbol{q}}(\boldsymbol{k})]^2\sin[\phi_0(\boldsymbol{k}) - 2\Phi^S_{\boldsymbol{q}}(\boldsymbol{k})] - [F^A_{\boldsymbol{q}}(\boldsymbol{k})]^2\sin[\phi_0(\boldsymbol{k}) - 2\Phi^A_{\boldsymbol{q}}(\boldsymbol{k})]\}
\end{aligned} \tag{S45}$$

We note that, the interaction-induced renormalization of the symmetric piece of the dispersion $h_{x,y}$ contains the symmetric form factor $F^S_{\boldsymbol{q}}(\boldsymbol{k})$ whereas the asymmetric piece h_0 contains at least one factor of the asymmetric form factor $F^A_{\boldsymbol{q}}(\boldsymbol{k})$. Thus our previous discussion (cf. Fig. S2) implies that $h_{x,y}$ is, on average, significantly larger than h_0. This is verified by plotting the values of $h_0(\boldsymbol{k})$ and $|h_x(\boldsymbol{k}) + ih_y(\boldsymbol{k})|$ ($h_{x,y}(\boldsymbol{k})$ are not separately gauge invariant) as a function of $\boldsymbol{k}$ as shown in Fig. S3. By averaging $|h_0(\boldsymbol{k})|$ and $|h_x(\boldsymbol{k}) + ih_y(\boldsymbol{k})|$, we can obtain an estimate for the energy scales associated with the symmetric and

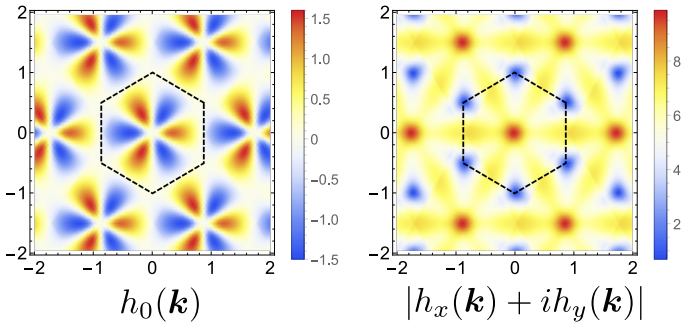

FIG. S3. The parameters of the renormalized dispersion defined in (S45). We notice that the chiral symmetric part $h_{x,y}(\boldsymbol{k})$ is much larger than the symmetry breaking part $h_0(\boldsymbol{k})$.

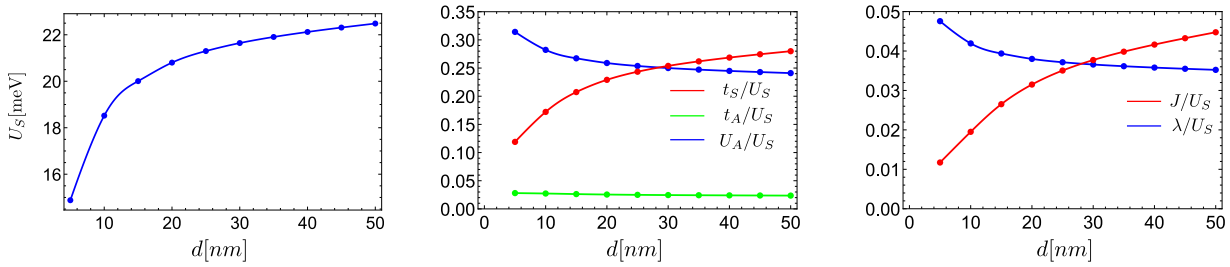

FIG. S4. Dependence of the different energy scales on the screening length d. The left panel shows the overall interaction scale in meV. The middle panel shows the strength of the symmetric dispersion t_S, symmetry-breaking interaction U_A, and symmetry-breaking dispersion t_A relative to the symmetric interaction scale U_S. The right panel shows the strength of the antiferromagnetic coupling J and the energy splitting of the ground state manifold due to the symmetry breaking interaciton λ.

symmetric breaking piece of the dispersion

$$t_S = \frac{1}{N}\sum_{\boldsymbol{k}} |h_x(\boldsymbol{k}) + ih_y(\boldsymbol{k})|, \qquad t_A = \frac{1}{N}\sum_{\boldsymbol{k}} |h_0(\boldsymbol{k})| \tag{S46}$$

leading to $t_S \approx 5$ meV and $t_A \approx 0.5$ meV.

The previous discussion implies that the intrasublattice part of the interaction $\mathcal{H}_S \sim 20$ meV is the largest scale in the problem. It is followed by the intersublattice part of the dispersion $h_{x,y}(\boldsymbol{k})$ and the intersublattice part of the interaction $\mathcal{H}_A$ which are of the same order ~ 5 meV which is about a factor of 4 smaller than $\mathcal{H}_S$. The non-symmetric part of the dispersion is much smaller ~ 0.5 meV.

3. *Dependence on screening*

Although the relative strength of the different parameters $U_{S/A}$, $t_{S/A}$ is insensitive to the overall strength of the interaction determined by the dielectric constant ϵ, it can be sensitive to the form of the interaction which is controlled by the screening length d which was shown to be tunable in recent experiments [13, 14] by tuning the distance to the metallic gate. Apart from the dependence of the overall interaction scale on the screening length d (left panel in Fig. S4), we can also see that the magnitude of the dispersion t_S and symmetry breaking interaction U_A relative to the symmetric interaction U_S depend weakly on the screening length. In particular, although both scales are always a factor of 3-5 smaller than the interaction, their relative strength depends on the screening, with the dispersion favored by larger screening length and the symmetry breaking interaction favored by smaller screening length.

4. Hierarchy of symmetries

The largest scale in the problem $\mathcal{H}_S$ is associated with an enlarged symmetry which can be seen by noting its invariance under any unitary transformation

$$c \mapsto Uc, \qquad [U, \sigma_z\tau_z] = 0 \tag{S47}$$

which yields the symmetry group U(4)×U(4) denoting independent rotations between states within a fixed Chern number sector.

The discussion of symmetry is simplified if we introduce the a new basis $\boldsymbol{\gamma}$ and $\boldsymbol{\eta}$ such that $\frac{1}{2}(1 \pm \gamma_z)$ projects onto the space of bands with Chern number ± 1 and $\boldsymbol{\eta}$ labels the states with the same spin within this subspace. This means the subspace of bands with $\gamma_z = 1$ consists of states polarized to sublattice A in the $+$ valley and sublattice B in the $-$ valley and vice versa for $\gamma_z = -1$ with $\boldsymbol{\eta}$ specifying the state within this 2-band subspace. More specifically, we define

$$\boldsymbol{\gamma} = (\sigma_x, \sigma_y\tau_z, \sigma_z\tau_z), \qquad \boldsymbol{\eta} = (\sigma_x\tau_x, \sigma_x\tau_y, \tau_z) \tag{S48}$$

In this basis, the symmetry of $\mathcal{H}_S$ is given by

$$U = \begin{pmatrix} U_1 & 0 \\ 0 & U_2 \end{pmatrix}_\gamma \tag{S49}$$

This symmetry is broken in two different ways. The intersublattice dispersion $h_{x,y}(\boldsymbol{k})$ breaks it down to $\mathrm{U}(4)$ by requiring U to commute with $\sigma_x = \gamma_x$ which is equivalent to the condition $U_1 = U_2$ in (S49) reducing the $\mathrm{U}(4) \times \mathrm{U}(4)$ symmetry of the interaction to $\mathrm{U}(4)$.

The other symmetry breaking effect comes from the intersublattice interaction $\mathcal{H}_A$ which reduces the symmetry of the interaction from $\mathrm{U}(4) \times \mathrm{U}(4)$ to $\mathrm{U}(4)$ by enforcing the extra condition that U commutes with $\sigma_x\tau_z = \eta_z\gamma_x$ leading to $U_1 = \eta_z U_2 \eta_z$. This $\mathrm{U}(4)$ subgroup is different from the $\mathrm{U}(4)$ subgroup leaving $h_{x,y}(\boldsymbol{k})$ invariant. In the presence of both $h_{x,y}(\boldsymbol{k})$ and $\mathcal{H}_A$, the symmetry is obtained by intersecting the two $\mathrm{U}(4)$ subgroups leading to $U_1 = U_2 = \eta_z U_1 \eta_z$ which implies

$$U_1 = U_2 = \begin{pmatrix} V_+ & 0 \\ 0 & V_- \end{pmatrix}_\eta \tag{S50}$$

This corresponds to $\mathrm{U}(2)_K \times \mathrm{U}(2)_{K'}$ symmetry corresponding to independent $\mathrm{U}(2)$ rotation within each valley. We notice that the much smaller intrasublattice dispersion h_0 does not introduce any extra symmetry breaking.

IV. SYMMETRIC STRONG COUPLING LIMIT

Motivated by the discussion of the previous section, we will now consider a strong coupling approach to the problem by assuming that the intrasublattice interaction scale is much larger than both the intersublattice interaction $\mathcal{H}_A$ and the intersublattice single-particle Hamiltonian $h_{x,y}$, i.e. $U_S \gg U_A, t_S$. Furthermore, we will neglect the intrasublattice dispersion h_0 since it is smaller than all other terms and does not break any symmetry that is unbroken at a higher energy scale.

A. Spinless model

For simplicity, let us first consider the simpler problem of spinless electrons at half-filling with the $\mathrm{U}(4) \times \mathrm{U}(4)$ symmetry replaced by $\mathrm{U}(2) \times \mathrm{U}(2)$. We start by noting that since $\delta\rho^S_{-\boldsymbol{q}} = [\delta\rho^S_{\boldsymbol{q}}]^\dagger$, the Hamiltonian $\mathcal{H}_S$ is a non-negative definite operator. As a result, any many-body state annihilated by $\mathcal{H}_S$ is a ground state [15, 16]. We further note that for any Slater determinant state $|\Psi_Q\rangle$ described by the density matrix $P(\boldsymbol{k}) = \frac{1}{2}(1 + Q)$ where Q commutes with $\sigma_z\tau_z$, the action of the Hamiltonian is given by

$$\mathcal{H}_S|\Psi_Q\rangle = 2NE_C|\Psi_Q\rangle, \qquad E_C = \frac{C_T^2}{AN}\sum_{\boldsymbol{G}} V_{\boldsymbol{G}} |\sum_{\boldsymbol{k}} F^S_{\boldsymbol{G}}(\boldsymbol{k}) \sin\Phi^S_{\boldsymbol{G}}(\boldsymbol{k})|^2 \tag{S51}$$

where C_T is the total Chern number of the state. In a periodic gauge, (S21) implies $\Lambda_{\boldsymbol{G}}(\boldsymbol{k}) = \Lambda^\dagger_{-\boldsymbol{G}}(\boldsymbol{k})$ which, together with (S34), implies that $\Phi^S_{\boldsymbol{G}}(\boldsymbol{k}) = -\Phi^S_{-\boldsymbol{G}}(\boldsymbol{k})$. As a result, the summation over $\boldsymbol{k}$ in E_C vanishes identically, leading to $\mathcal{H}_S|\Psi_Q\rangle = 0$. Thus, we see that the states $|\Psi_Q\rangle$ with Q commuting with $\sigma_z\tau_z$ are exact ground states of $\mathcal{H}_S$.

These states can be understood using the schematic illustration of Fig. 3 in the main text. The figure contains four bands labelled by valley and sublattice indices and since the symmetric form factor $\Lambda^S_{\boldsymbol{q}}(\boldsymbol{k})$ is diagonal in both, the interaction $\mathcal{H}_S$ is minimized by minimizing density fluctuations within each band which is achieved by completely filling two of the four bands. There are several possible ways to do this which can be grouped into two categories: (i) filling two bands with the same Chern number leading to a $C_T = \pm 2$ QH states which is invariant under $\mathrm{U}(2) \times \mathrm{U}(2)$, or (ii) filling two states with opposite Chern number leading to a manifold of $C_T = 0$ states generated by acting with $\mathrm{U}(2) \times \mathrm{U}(2)$ on the VP state $Q = \tau_z$.

1. *Effect of $h_{x,y}$*

Next, we consider the effect of the dispersion $h_{x,y}(\boldsymbol{k})$ on this manifold of states. This breaks the symmetry down to $\mathrm{U}(2)$ by coupling pairs of bands with opposite Chern number through tunneling with amplitude $h_x(\boldsymbol{k}) + ih_y(\boldsymbol{k})$. This can be seen by noting that the symmetric dispersion has the form $\gamma_x h_x(\boldsymbol{k}) + \gamma_y h_y(\boldsymbol{k})$, thus, in the γ, η basis, it connects bands with opposite $\gamma_z = \pm 1$ with the same value of η_z.

We first note that, among the manifold of ground states of $\mathcal{H}_S$, those for which Q commutes with σ_x are annihilated by $h_{x,y}$. These correspond to states in which each pair of bands connected by the tunelling in Fig. 4 are both either filled or empty, forming the manifold $\mathrm{U}(2)/\mathrm{U}(1) \times \mathrm{U}(1) \simeq S^2$ spanned by the VP state $Q = \tau_z$ and $\mathcal{T}$-IVC. To understand the action of $h_{x,y}$, let us first consider the case in which Q anticommutes with $h_{x,y}$ corresponding to states for which only one out of each pair of coupled bands in Fig. 4 is filled. The action of $h_{x,y}$ on such states creates an electron-hole pair by moving an electron at momentum $\boldsymbol{k}$ from a filled band to the same momentum at the corresponding empty band with opposite Chern number.

The energy associated with such process can be calculated within second order perturbation theory where an electron-hole pair is created then annihilated. Since this can be done for each pair of bands independently, we can limit ourselves to only one pair of bands with opposite Chern number coupled by $h_{x,y}$ which can be labelled with $C = \sigma_z \tau_z = \gamma_z = \pm 1$. We denote a state with an electron-hole pair with momentum $\boldsymbol{k}$ by

$$|\Psi_{\boldsymbol{k},\mathrm{eh}}\rangle = c^\dagger_{\boldsymbol{k},-} c_{\boldsymbol{k},+} |\Psi_+\rangle, \qquad |\Psi_+\rangle = \prod_{\boldsymbol{k}} c^\dagger_{\boldsymbol{k},+} |0\rangle \tag{S52}$$

where $|\Psi_+\rangle$ is the state where the $C = +1$ band is filled and the $C = -1$ band is empty. The energy correction (per particle) due to the coupling $h_x(\boldsymbol{k}) + ih_y(\boldsymbol{k})$ between the two bands is then given by

$$\Delta E = -J = -\frac{1}{N} \sum_{\boldsymbol{k},\boldsymbol{k}'} [h_x(\boldsymbol{k}) + ih_y(\boldsymbol{k})][\mathcal{H}^{-1}_{\mathrm{eh}}]_{\boldsymbol{k},\boldsymbol{k}'} [h_x(\boldsymbol{k}') - ih_y(\boldsymbol{k}')], \qquad [\mathcal{H}_{\mathrm{eh}}]_{\boldsymbol{k},\boldsymbol{k}'} = \langle \Psi_{\boldsymbol{k},\mathrm{eh}} | \mathcal{H}_S | \Psi_{\boldsymbol{k}',\mathrm{eh}} \rangle \tag{S53}$$

We note that operator $\mathcal{H}_S$ conserves the number of electron-hole pairs and their momentum so it acts within the space of states $|\Psi_{\boldsymbol{k},\mathrm{eh}}\rangle$. As a result, $\mathcal{H}_{\mathrm{eh}}$ is given by

$$[\mathcal{H}_{\mathrm{eh}}]_{\boldsymbol{k},\boldsymbol{k}'} = \frac{1}{A} \sum_{\boldsymbol{q}} V_{\boldsymbol{q}} |F^S_{\boldsymbol{q}}(\boldsymbol{k})|^2 \{\delta_{\boldsymbol{k},\boldsymbol{k}'} - \delta_{\boldsymbol{k}',[\boldsymbol{k}+\boldsymbol{q}]} e^{2i\phi_{\boldsymbol{q}}(\boldsymbol{k})}\} \tag{S54}$$

where $[\boldsymbol{q}]$ denotes the part of $\boldsymbol{q}$ within the first zone. This expression can be understood by noting that the action of $\delta\rho^S_{\boldsymbol{q}}$ on an electron-hole pair either increases the momentum of the electron by $\boldsymbol{q}$ or decreases the momentum of the hole by $\boldsymbol{q}$. As a result, the action of $\delta\rho^S_{-\boldsymbol{q}} \delta\rho^S_{\boldsymbol{q}}$ either returns the electron-hole pair to its initial state or shifts both momenta by $\pm\boldsymbol{q}$. The matrix $\mathcal{H}_{\mathrm{eh}}$ can be easily evaluated numerically leading to $J \approx 1.5$ meV. This agrees with the simple estimate which assumes that the typical value for the eigenvalues of $\mathcal{H}_{\mathrm{eh}}$ are of the same order as the interaction scale 15-20 meV, yielding $J \approx t_S^2/U_S$ 1-3 meV. The dependence of J on the screening is shown in Fig. S4. We can see that the antiferromagnetic coupling increases with increasing the screening length due to the increase in the dispersion renormalized dispersion t_S.

One important observation that is crucial for the previous argument is that the spectrum of the electron-hole pairs has a gap. This feature can be traced to the band topology as follows. We start by writing a general state with a single electron-hole pair

$$|\Psi_{\mathrm{eh}}\rangle = \frac{1}{\sqrt{N}} \sum_{\boldsymbol{k}} a_{\boldsymbol{k}} |\Psi_{\boldsymbol{k},\mathrm{eh}}\rangle, \qquad \sum_{\boldsymbol{k}} |a_{\boldsymbol{k}}|^2 = N \tag{S55}$$

We note that restricting this sum to the first Brillouin zone requires $a_{\boldsymbol{k}} c^\dagger_{\boldsymbol{k},-} c_{\boldsymbol{k},+}$ to be periodic in $\boldsymbol{k}$. Due to band topology, it is impossible to choose a smooth and periodic gauge. In the following discussion, we will prefer to choose a smooth gauge for which the operators $c_{\boldsymbol{k},\pm}$ are not periodic in $\boldsymbol{k}$. Instead, their phase winds by $\pm 2\pi$ around the Brillouin zone. As a result, the phase of $a_{\boldsymbol{k}}$ should wind by 4π around the Brillouin zone, i.e. $a_{\boldsymbol{k}}$ has at least two vortices.

Substituting in (S54), we get

$$\langle\Psi_{\rm eh}|\mathcal{H}_{\rm eh}|\Psi_{\rm eh}\rangle = \frac{1}{AN}\sum_{\boldsymbol{k},\boldsymbol{q}} V_{\boldsymbol{q}}[F^S_{\boldsymbol{q}}(\boldsymbol{k})]^2[|a_{\boldsymbol{k}}|^2 - e^{2i\Phi_{\boldsymbol{q}}(\boldsymbol{k})}a^*_{\boldsymbol{k}+\boldsymbol{q}}a_{\boldsymbol{k}}] \tag{S56}$$

We now notice that to leading order in $\boldsymbol{q}$, $\Phi^S_{\boldsymbol{q}}(\boldsymbol{k})$ can be written as $\Phi^S_{\boldsymbol{q}}(\boldsymbol{k}) = -\boldsymbol{q}\cdot\boldsymbol{A}_{\boldsymbol{k}} + O(\boldsymbol{q}^3)$ where $\boldsymbol{A}_{\boldsymbol{k}}$ is the Berry connection

$$\boldsymbol{A} = -i\langle u_{\boldsymbol{k}}|\nabla|u_{\boldsymbol{k}}\rangle, \qquad \frac{1}{2\pi}\int_{\rm BZ}\nabla_{\boldsymbol{k}}\times\boldsymbol{A}_{\boldsymbol{k}} = 1 \tag{S57}$$

To make further analytical progress, we assume that the magnitude of the form factor $F^S_{\boldsymbol{q}}(\boldsymbol{k})$ depends only on $|\boldsymbol{q}|$ and decays relatively quickly in $\boldsymbol{q}$ on the scale of the Brillouin zone leading to

$$\begin{aligned}\langle\Psi_{\rm eh}|\mathcal{H}_{\rm eh}|\Psi_{\rm eh}\rangle &= \frac{c}{N}\sum_{\boldsymbol{k}}|(\nabla_{\boldsymbol{k}} - 2i\boldsymbol{A}_{\boldsymbol{k}})a_{\boldsymbol{k}}|^2 = c\int_{\rm BZ}\frac{d^2\boldsymbol{k}}{(2\pi)^2}|(\nabla_{\boldsymbol{k}} - 2i\boldsymbol{A}_{\boldsymbol{k}})a_{\boldsymbol{k}}|^2,\\ c &= \frac{1}{2A}\sum_{\boldsymbol{q}\neq\boldsymbol{G}}\boldsymbol{q}^2V_{\boldsymbol{q}}|F^S_{\boldsymbol{q}}|^2 = \frac{1}{2}\int\frac{d^2\boldsymbol{q}}{(2\pi)^2}\boldsymbol{q}^2V_{\boldsymbol{q}}|F^S_{\boldsymbol{q}}|^2\end{aligned} \tag{S58}$$

where c is the constant of the same order as the interaction scale. We note that (S58) has the same form as the Ginzburg-Landau free energy of a superconductor in a magnetic field in momentum space which is in the vortex lattice phase with two vortices per unit cell due to the non-trivial winding of $a_{\boldsymbol{k}}$. The free energy of such phase is always larger than zero which can be seen by employing similar arguments to those of Ref. [17] as shown below.

We start with the observation that, in a smooth non-singular gauge, $\boldsymbol{A}_{\boldsymbol{k}}$ is finite everywhere in the Brillouin zone $|\boldsymbol{A}_{\boldsymbol{k}}| \leq |\boldsymbol{A}_{\boldsymbol{k},\max}|$. Without loss of generality, we can write $a_{\boldsymbol{k}} = \rho(k_x + ik_y)$ close to a vortex. If we choose a ball of radius $\epsilon \ll |\boldsymbol{A}_{\boldsymbol{k},\max}|^{-1}$ around the vortex, then its energy is given by $\frac{c}{\pi}\rho^2\epsilon^2[1 + O(\epsilon^2|\boldsymbol{A}_{\boldsymbol{k},\max}|^2)]$ which is always finite since ρ cannot be made arbitrarily small (this is a result of the normalization constraint (S55)). As a result, the energy expectation value in (S58) is always positive, i.e. the Hamiltonian $\mathcal{H}_{\rm eh}$ is gapped.

In summary, $h_{x,y}$ favors states where only one from each pair of bands connected by $h_{x,y}$ is filled, allowing for virtual hopping which lowers their energy by an amount $J \sim t_S/U_S$. This is equivalent to the condition $\{Q, \sigma_x\}$ which selects a manifold of states consisting of two sectors: a $\mathrm{U}(2)$-invariant QH state with Chern number ± 2 and a manifold of states with vanishing Chern number corresponding to $\mathrm{U}(2)/\mathrm{U}(1)\times\mathrm{U}(1) \simeq S^2$ generated by the VH and K-IVC states.

2. *Effect of $\mathcal{H}_A$*

The intersublattice interaction $\mathcal{H}_A$, on the other hand, picks a different submanifold of ground states corresponding to the states annihilated by the non-symmetric density operator $\delta\rho^A_{\boldsymbol{q}}$. These are characterized by Q which commutes with σ_y forming the manifold $\mathrm{U}(2)/\mathrm{U}(1)\times\mathrm{U}(1) \simeq S^2$ generated by the VP and K-IVC. The energies of the remaining states for which Q anticommutes with σ_y (QH, VH, and $\mathcal{T}$-IVC) are increased by an amount of the order

$$\lambda = \frac{1}{2AN}\sum_{\boldsymbol{k},\boldsymbol{q}} V_{\boldsymbol{q}}|F^A_{\boldsymbol{q}}(\boldsymbol{k})|^2 \approx 0.5\text{meV}. \tag{S59}$$

The dependence of λ on the screening is shown in Fig. S4. We can see that it remains relative constant except for very small values of screening where it starts slightly increasing.

Thus, in the presence of both $h_{x,y}$ and $\mathcal{H}_A$, the K-IVC, which benefits from both perturbations, has the lowest energy followed by the VP and QH/VH (the latter two are degenerate) whose competition is determined by the relative strength of the symmetry-breaking terms in the interaction λ and the energy gain due to virtual tunneling $-J$. The $\mathcal{T}$-IVC state, which was not seen in the numerics, is disfavored by both and has the highest energy.

B. Spinful model

1. Charge neutrality

Upon including the spin, we can study the manifold of ground states at CN in a similar fashion starting with the states which minimize $\mathcal{H}_S$ for which Q commutes with $\sigma_z\tau_z$. These states are obtained by completely filling 4 of the 8 bands in Fig. 3. There are three sectors of such states with Chern numbers ±4, ±2 and 0. The manifold of Chern number ±4 consists of a single state $Q = \sigma_z\tau_z$ invariant under $\mathrm{U}(4) \times \mathrm{U}(4)$ rotations which is the analog of the QH state in the spinless case. The manifold of states with Chern number ±2 is obained by filling three bands with one Chern number and a single band with the opposite Chern number. This manifold is 12-dimensional and is isomorphic to $[\mathrm{U}(4)/\mathrm{U}(3) \times \mathrm{U}(1)]^2$. The states within this manifold break several symmetries and are characterized by mixed orders where, for instance, one valley has a spin-polarized state whereas the other has a $C_2\mathcal{T}$-breaking sublattice polarized state. They necessarily involve some non-trivial spin structure and do not have analogs in the spinless problem. Finally, the manifold of zero Chern number states is 16-dimensional and is isomorhphic to $[\mathrm{U}(4)/\mathrm{U}(2) \times \mathrm{U}(2)]^2$. This manifold includes all the zero Chern number states found in the spinless model (VH, VP, $\mathcal{T}$-IVC, and K-IVC) in their spin-singlet $Q \propto s_0$ or spin-triplet $Q \propto \boldsymbol{n} \cdot \boldsymbol{s}$ variants. It also includes the purely spin-polarized (SP) state $Q = \boldsymbol{n} \cdot \boldsymbol{s}$.

The dispersion $h_{x,y}$ selects for the states where only one band out of each pair of bands coupled by $h_{x,y}$ is filled which is equivalent to the requirement that Q anticommutes with σ_x. This reduces the manifold of state with Chern number ±2 to a 6-dimensional manifold $\mathrm{U}(4)/\mathrm{U}(3) \times \mathrm{U}(1)$ and that of Chern number 0 states to an 8-dimensional manifold $\mathrm{U}(4)/\mathrm{U}(2) \times \mathrm{U}(2)$. The latter includes the VH and K-IVC states (both spin-singlet and triplet versions) but does not include the SP, VP or $\mathcal{T}$-IVC states.

The non-symmetric interaction $\mathcal{H}_A$ selects a different submanifold of states with the requirement that Q commutes with $\sigma_x\tau_z$. The possible states satisfying this requirement has Chern numbers ±2 or 0 with the former forming the 6-dimensional manifold $\mathrm{U}(4)/\mathrm{U}(3) \times \mathrm{U}(1)$ and the latter forming 8-dimensional manifold $\mathrm{U}(4)/\mathrm{U}(2) \times \mathrm{U}(2)$. The zero Chern number states include the VP, SP, and K-IVC states.

Thus, the presence of both h_{xy} and $\mathcal{H}_A$ selects the K-IVC state as the unique ground state up to the action of $\mathrm{U}(2)_K \times \mathrm{U}(2)_{K'}$ symmetry corresponding to independent spin rotation in each valley. The most general K-IVC state is given by

$$Q = \sigma_y \otimes \begin{pmatrix} 0 & V \\ V^\dagger & 0 \end{pmatrix}_\tau \tag{S60}$$

where V is a 2×2 unitary matrix acting in the spin space. The gound state manifold is thus isomorphic to $\mathrm{U}(2)$. The action of $\mathrm{U}(2) \times \mathrm{U}(2)$ symmetry on the ground state is

$$V \mapsto U_+^\dagger V U_- \tag{S61}$$

which generates the full $\mathrm{U}(2)$ group starting from any given state , e.g. $V = 1$. This means that any given state is invariant under a $\mathrm{U}(2)$ subgroup given by the condition $U_- = V^\dagger U_+ V$ which is consistent with the ground state manifold being $\mathrm{U}(2) \simeq \frac{\mathrm{U}(2)\times\mathrm{U}(2)}{\mathrm{U}(2)}$. This manifold which can be written as $\mathrm{U}(1) \times \mathrm{SU}(2)$ can be parametrized as $e^{i\phi}e^{i\frac{\theta}{2}\boldsymbol{n}\cdot\boldsymbol{s}}$, $0 \le \phi < 2\pi$, $0 \le \theta \le \pi$. Here, ϕ and θ can be associated with the total and relative angles of the IVC orders in the spin up and down sectors.

In the presence of intervalley Hund's term given by

$$\mathcal{H}_J = \frac{J}{N}\boldsymbol{S}_{+,\boldsymbol{q}} \cdot \boldsymbol{S}_{-,-\boldsymbol{q}}, \qquad \boldsymbol{S}_{\pm,\boldsymbol{q}} = \sum_{\boldsymbol{k}} c_{\boldsymbol{k}}^\dagger \frac{1 \pm \tau_z}{2} \boldsymbol{s} c_{\boldsymbol{k}+\boldsymbol{q}} \tag{S62}$$

the $\mathrm{U}(2)_K \times \mathrm{U}(2)_{K'}$ symmetry is broken down to $\mathrm{U}_C(1) \times \mathrm{U}_V(1) \times \mathrm{SU}(2)$. For the ground state Q parametrized by ϕ, θ and $\boldsymbol{n}$, we note that the energy should remain independent on ϕ and $\boldsymbol{n}$ since they still transform non-trivially under the symmetry. Thus, we can fix their value to $\phi = 0$ and $\boldsymbol{n} = \hat{z}$. We now evaluate $E_J(\theta) = \langle\Psi_\theta|\mathcal{H}_J|\Psi_\theta\rangle$ which is nothing but the Hartree-Fock decoupling of $\mathcal{H}_J$. The Hartree term vanishes whereas the Fock term yields (up to a constant)

$$E_J(\theta) \propto -J \sum_a \mathrm{tr}\, e^{i\frac{\theta}{2}s_z} s^a e^{-i\frac{\theta}{2}s_z} s^a = -2J(1 + 2\cos\theta) \tag{S63}$$

For ferromagnetic Hund $J < 0$, the minimum is at $\theta = \pi$ while for antiferromagnetic Hund $J > 0$, the minimum is at $\theta = 0$.

2. Half-filling

The ground state at half-filling $\nu = \pm 2$ can be understood similarly. In the following, we will focus on the case $\nu = -2$. The $\nu = 2$ case is very similar. At $\nu = -2$, Q satisfies $\mathrm{tr}\, Q = -4$ and can be generally written as

$$Q = -P_- + P_+ Q_1, \qquad P_\pm = \frac{1}{2}(1 \pm Q_2), \qquad Q_{1,2}^2 = 1, \quad \mathrm{tr}\, Q_{1,2} = 0, \quad [Q_1, Q_2] = 0 \tag{S64}$$

This describes a state where the 4 bands associated with the projector P_- are completely empty, whereas the 4 bands associated with the projector P_+ are half-filled.

The analysis of the ground state manifold is very similar to the CN case. We start by the states which minimize $\mathcal{H}_S$ which are specified by requiring $[Q_{1,2}, \sigma_z \tau_z] = 0$. This is equivalent to filling 2 out of the 8 bands of Fig. 4. The manifold of ground state consists of two sectors depending on whether the two filled bands have the same Chern number. The first sector contains Chern number 2 states such as spin-polarized QH state $Q_2 = s_z$, $Q_1 = \sigma_z \tau_z$ which form the manifold $\mathrm{U}(4)/\mathrm{U}(2) \times \mathrm{U}(2)$. The second sector contains Chern number 0 states such as spin-polarized VH state $Q_2 = s_z$, $Q_1 = \sigma_z$ or spin and valley polarized states $Q_2 = s_z$, $Q_1 = \tau_z$ which form the manifold $[\mathrm{U}(4)/\mathrm{U}(3) \times \mathrm{U}(1)]^2$.

Including $h_{x,y}$ selects states for which at most one band from each pair connected by the tunneling $h_{x,y}$ is filled. This is equivalent to the condition $[Q_2, \sigma_x] = 0$, $\{Q_1, \sigma_x\} = 0$. All states with Chern number 2 are included in this manifold. For the zero Chern number sector, this selects a submanifold of states isomorphic to $\mathrm{U}(4)/\mathrm{U}(3) \times \mathrm{U}(1)$. The non-symmetric part of the interaction $\mathcal{H}_A$ instead requires states related by the action of $\sigma_x \tau_z$ to be both filled or both empty. This is equivalent to the condition $[Q_{1,2}, \sigma_x \tau_z] = 0$. This condition rules out all states with non-vanishing Chern number and it selects a submanifold of zero Chern number states isomorphic to $\mathrm{U}(4)/\mathrm{U}(3) \times \mathrm{U}(1)$.

The two constraints are only simultaneously satisfied by K-IVC states. The simplest such state at half-filling is the spin-polarized IVC state obtained by taking $Q_2 = s_z$ and $Q_1 = \sigma_y(\tau_+ e^{i\phi} + \tau_- e^{i\phi})$. The manifold of ground state is generated by acting with $\mathrm{U}(2)_K \times \mathrm{U}(2)_{K'}$ on this state yielding

$$Q = \begin{pmatrix} \frac{1}{2}(1 + \boldsymbol{n}_+ \cdot \boldsymbol{s}) & \Xi \sigma_y \\ \Xi^\dagger \sigma_y & \frac{1}{2}(1 + \boldsymbol{n}_- \cdot \boldsymbol{s}) \end{pmatrix}_\tau, \qquad \boldsymbol{n}_\pm = \frac{1}{2}\,\mathrm{tr}\, U_\pm^\dagger s_z U_\pm \boldsymbol{s}, \qquad \Xi = U_+^\dagger P_\downarrow U_-, \qquad P_{\uparrow/\downarrow} = \frac{1 \pm s_z}{2} \tag{S65}$$

where U_+, and U_- are 2×2 matrices acting in spin space. This state is parametrized by U_+ and U_-. However, we note that the replacement $U_\pm \mapsto e^{i(\phi_\pm P_\downarrow + \phi P_\uparrow)} U_\pm$ for any phases ϕ, ϕ_+ and ϕ_- does not change the state Q. Thus, Q parametrizes the manifold $\frac{\mathrm{U}(2)\times\mathrm{U}(2)}{\mathrm{U}(1)\times\mathrm{U}(1)\times\mathrm{U}(1)} \simeq \mathrm{U}(1) \times S^2 \times S^2$. Here, the $\mathrm{U}(1)$ denotes the IVC phase and the two S^2 factors denote the spin direction in each valley. Such states denotes a spin polarized IVC with the spin direction in each valley chosen independently.

The intervalley Hund's coupling will select the state where the spin is aligned in both valleys for $J < 0$ which can be implemented by taking $U_+ = e^{i\phi} U_-$. For $J > 0$, it will select the spin-valley-locked state where spins are anti-aligned in the two valleys. This is implemented by the choice $U_+ = s_x e^{i\phi} U_-$.

[S1] R. Bistritzer and A. H. MacDonald, Proceedings of the National Academy of Sciences **108**, 12233 (2011).
[S2] H. C. Po, L. Zou, A. Vishwanath, and T. Senthil, Phys. Rev. X **8**, 031089 (2018).
[S3] H. C. Po, L. Zou, T. Senthil, and A. Vishwanath, Physical Review B **99** (2019), 10.1103/physrevb.99.195455.
[S4] J. Ahn, S. Park, and B.-J. Yang, Physical Review X **9**, 021013 (2019), arXiv:1808.05375 [cond-mat.mes-hall].
[S5] Z. Song, Z. Wang, W. Shi, G. Li, C. Fang, and B. A. Bernevig, Phys. Rev. Lett. **123**, 036401 (2019).
[S6] S. Liu, E. Khalaf, J. Y. Lee, and A. Vishwanath, arXiv preprint arXiv:1905.07409 (2019).
[S7] M. Xie and A. H. MacDonald, arXiv preprint arXiv:1812.04213 (2018).
[S8] J. Jung and A. H. MacDonald, Phys. Rev. B **89**, 035405 (2014).
[S9] E. Cancès and C. Le Bris, International Journal of Quantum Chemistry **79**, 82 (2000).
[S10] K. N. Kudin, G. E. Scuseria, and E. Cancès, The Journal of Chemical Physics **116**, 8255 (2002).
[S11] G. Tarnopolsky, A. J. Kruchkov, and A. Vishwanath, Phys. Rev. Lett. **122**, 106405 (2019).
[S12] C. Fang, M. J. Gilbert, and B. A. Bernevig, Phys. Rev. B **86**, 115112 (2012).
[S13] P. Stepanov, I. Das, X. Lu, A. Fahimniya, K. Watanabe, T. Taniguchi, F. H. Koppens, J. Lischner, L. Levitov, and D. K. Efetov, arXiv preprint arXiv:1911.09198 (2019).
[S14] Y. Saito, J. Ge, K. Watanabe, T. Taniguchi, and A. F. Young, arXiv preprint arXiv:1911.13302 (2019).
[S15] C. Repellin, Z. Dong, Y.-H. Zhang, and T. Senthil, arXiv preprint arXiv:1907.11723 (2019).
[S16] Y. Alavirad and J. D. Sau, arXiv preprint arXiv:1907.13633 (2019).
[S17] N. Bultinck, S. Chatterjee, and M. P. Zaletel, arXiv preprint arXiv:1901.08110 (2019).